Monthly Notices
of the
ROYAL ASTRONOMICAL SOCIETY

MNRAS **472,** 4007–4012 (2017)
Advance Access publication 2017 August 31

doi:10.1093/mnras/stx2236

Probing the properties of the pulsar wind via studying the dispersive effects in the pulses from the pulsar companion in a double neutron-star binary system

Shu-Xu Yi★ and K.-S. Cheng★

Department of Physics, The University of Hong Kong, Pokfulam Road, Hong Kong

Accepted 2017 August 25. in original form 2017 August 23

ABSTRACT

The velocity and density distribution of $e^{\pm}$ in the pulsar wind are crucial distinction among magnetosphere models, and contain key parameters determining the high-energy emission of pulsar binaries. In this work, a direct method is proposed, which might probe the properties of the wind from one pulsar in a double-pulsar binary. When the radio signals from the first-formed pulsar travel through the relativistic $e^{\pm}$ flow in the pulsar wind from the younger companion, the components of different radio frequencies will be dispersed. It will introduce an additional frequency-dependent time-of-arrival delay of pulses, which is function of the orbital phase. In this paper, we formulate the above-mentioned dispersive delay with the properties of the pulsar wind. As examples, we apply the formula to the double-pulsar system PSR J0737−3039A/B and the pulsar-neutron star binary PSR B1913+16. For PSR J0737−3039A/B, the time delay in 300 MHz is $\lesssim 10\,\mu\,s^{-1}$ near the superior conjunction, under the optimal pulsar wind parameters, which is approximately half of the current timing accuracy. For PSR B1913+16, with the assumption that the neutron-star companion has a typical spin-down luminosity of 10^{33} erg s^{-1}, the time delay is as large as $10 - 20\,\mu\,s^{-1}$ in 300 MHz. The best timing precision of this pulsar is $\sim 5\,\mu\,s^{-1}$ in 1400 MHz. Therefore, it is possible that we can find this signal in archival data. Otherwise, we can set an upper limit on the spin-down luminosity. Similar analysis can be applied to other 11 known pulsar-neutron star binaries.

Key words: binaries: general – pulsars: general.

1 INTRODUCTION

For its simplicity and intuitiveness, the vacuum magneto-dipole energy loss formula,

$$W_{\rm tot}^{\rm (V)} = \frac{1}{6}\frac{B_0^2\Omega^4R^6}{c^3}\sin^2\chi, \quad (1)$$

is still widely used as a rule of thumb to account for the braking of the spin-powered pulsars (see Lorimer & Kramer 2012, for instance). Although it has been known for a long time (see Beskin, Gurevich & Istomin 1983 and references therein) that the magnetodipole radiation should be fully screened by the magnetospheric plasma. More and more people believe that the pulsar wind takes away most of the rotational energy of the pulsar to infinity (Michel 1969; Tong et al. 2013; Li et al. 2014; Tong 2016). The pulsar wind is composed of electromagnetic waves (EMWs) and particles (mainly electrons/positions, $e^{\pm}$). The ratio between the energy fluxes of them is defined as the magnetization parameter $\sigma = W_{\rm EM}/W_{\rm part}$.

Studies with magnetohydrodynamic theory demonstrated that particles cannot be effectively accelerated in pulsar wind (Usov 1975; Melatos & Melrose 1996; Beskin, Kuznetsova & Rafikov 1998; Chiueh, Li & Begelman 1998; Bogovalov & Tsinganos 1999; Bogovalov 2001; Lyubarsky & Eichler 2001; Lyubarsky 2002), therefore $\sigma \gg 1$. However, large kinetic energy of $e^{\pm}$ in pulsar wind is needed in modelling the observations in high energy. Kennel & Coroniti (1984) explained the luminosity of the Crab nebula to be powered by the relativistic $e^{\pm}$ from the centre pulsar. A large kinetic energy in particles is required and thus $\sigma \ll 1$ is implied. In gamma-ray pulsar binaries, a large kinetic energy in particles is also crucial in explanation of the high-energy emissions. In those models, the pulsar wind needs to collide with the stellar wind to form a termination shock front, which accounts for the KeV X-ray and TeV gamma-ray emissions (e.g. in PSR B1259+63; Hirayama et al. 1999; Kirk, Ball & Skjæraasen 1999; Aharonian et al. 2005; Chernyakova et al. 2006; Kong et al. 2011; see also Dubus 2015 for a review). GeV emissions are modelled

★ E-mail: yishuxu@hku.hk (S-XY); hrspksc@hku.hk (K-SC)

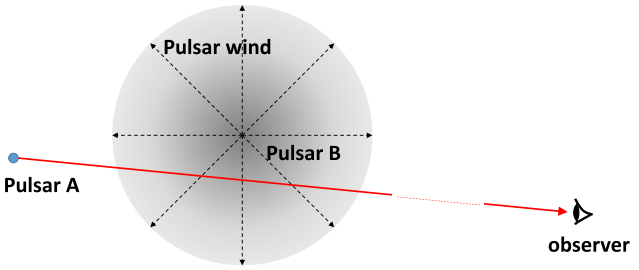

Figure 1. The illustration of additional DM of one pulsar from the pulsar wind from the other pulsar in a double-pulsar system.

as outcomes of inverse Compton scattering by the cold $e^{\pm}$ in the pulsar wind (Dubus & Cerutti 2013; Yi & Cheng 2017). The conflict between the needs of large kinetic energy of particles in the pulsar wind, and the difficulty in effective particle acceleration, is known as the 'σ-problem' (Beskin 2016).

To understand how the energy is dissipated from the Poynting flow to particles, i.e. to solve the σ-problem, has the merit for both the magnetosphere theories and for modelling the interaction between the pulsar and surrounding materials.

Since 1999 (Bogovalov 1999; Bogovalov & Tsinganos 1999; Contopoulos, Kazanas & Fendt 1999), studies have been refining the understanding of the magnetosphere and making progress towards the solution of the problem (see for instances Kirk & Skjæraasen 2003; Spitkovsky 2006; Bogovalov 2014). A satisfactory theory of magnetosphere is essential for modelling pulsar braking, which is the main cause of pulsar timing noises (Hobbs, Lyne & Kramer 2010). Reducing the timing noise is the major stream of efforts in pulsar timing, so as to unveil small signals such as gravitational waves (Arzoumanian et al. 2016; Babak et al. 2016; Yi & Zhang 2016; Zhu et al. 2016). Observational constraints on the density and velocity distribution of $e^{\pm}$ in pulsar wind can test and select among these theories of magnetosphere.

On the other hand, as mentioned above, in models explaining the emission from pulsar nebulae and gamma-ray pulsar binaries, the energy conversion process from EMW to particles is always considered phenomenally by σ as a function of the distance to the pulsar (as in Kong et al. 2011):

$$\sigma = \sigma_{\rm L}\left(\frac{r}{r_{\rm L}}\right)^{-\alpha_\sigma}, \tag{2}$$

where $r_{\rm L}$ is the radius of the light cylinder, and $\sigma_{\rm L}$ and α_σ are free parameters to be fitted to observations.

Therefore, an independent way to study the σ–r relationship is wanted, which can help to rule out some of the proposed models, and reduce the degree of freedom in other models.

Double-pulsar binary systems provide a possible method to study the above-mentioned question. $e^{\pm}$ in the pulsar wind from one of the pulsar (pulsar B) acts as a dispersive medium, when the radio pulsations from the other pulsar in the binary (pulsar A) travel through it. The line of sight from pulsar A to the Earth probes different depth in the pulsar wind at different orbital phases (see illustration in Fig. 1). Observation of the orbital phase-modulated dispersive effects in the signal of pulsar A can, in principle, serve as a way to study the density and velocity distribution of $e^{\pm}$ in the pulsar wind. When the bulk velocity of the $e^{\pm}$ is non-relativistic, the dispersion is determined solely by the density of $e^{\pm}$. When the medium becomes relativistic, the Lorentz factor of the bulk motion is also involved in the dispersion relationship. In Section 2, we study how the density and Lorentz factor distribution of $e^{\pm}$ in the pulsar wind determine the additional dispersion measure (DM) of the pulses from pulsar A. We also show the time delay of the pulse arrival time (TOA) due to this additional DM. In Section 3, we apply our formula into two realistic binary systems: PSR J0737−3039A/B and J1915+1606. PSR J0737−3039A/B is the only known double-pulsar binary. There are 13 pulsar binary systems in which the companion is likely to be a neutron star (double neutron stars or DNS; see the catalogue in Yang et al. 2017). These invisible neutron-star companions can be pulsars whose radiating beams miss the line of sight. We choose the famous Hulse–Taylor binary (Hulse & Taylor 1975, also known as PSR J1915+1606 or B1913+16) as an example of the potential intrinsic double-pulsar binaries. We show that pulsar timing observations that unveil such TOA variation signals can serve to determine the σ–r relationship. In Section 4, we discuss limits of practicability under the current radio telescope capabilities, and the further aspects of this proposed method. We conclude the paper in Section 5 and discuss in Section 6.

2 THEORY

In a double-pulsar system, the radio emissions from pulsar A travel through the wind zone of pulsar B and are dispersed. In order to describe the dispersion process, we define the following quantities and angles: a is the distance between pulsars A and B; α is the angle between the vector from pulsar A to B and the vector from pulsar A to the Earth; l denotes the distance from pulsar A to some point in the line of sight to the Earth; θ is the angle between the wind velocity and the propagating direction of the signals from A at that point (see Fig. 1 for illustration).

We derive the refractive index n_ν (defined as the group velocity of EMW in the vacuum c divided by that in the medium $c_{\rm g}$, $n_\nu \equiv c/c_{\rm g}$) of a stream of cold plasma with bulk velocity βc as follows.

The Lorentz transformation of three-dimensional velocity is

$$u' = \frac{\sqrt{u^2+\beta^2c^2-2\beta cu\cos\theta-\beta^2u^2\sin^2\theta}}{1-\beta u\cos\theta/c}. \tag{3}$$

In our case, the u is specified to $c_{\rm g}$. As definition, $c/c'_{\rm g} = n'_{\nu'}$ is the refractive index in the stream comoving frame (we will omit the prime mark over the subscript ν in the following text for pithiness), and $c/c_{\rm g} = n_\nu$ is the refractive index in the frame of the binary's barycentre. Square equation (3), and note that

$$1/n'_\nu = \sqrt{1-\nu_{\rm p}^2/\nu'^2}$$

($\nu_{\rm p}$ is the plasma frequency to be defined below), we have the equation about n_ν:

$$\frac{n_\nu^2-1}{(n_\nu-\beta\cos\theta)^2} = \left(\frac{\nu_{\rm p}}{\nu}\right)^2\frac{1}{(1-\beta\cos\theta)^2}. \tag{4}$$

Solve the above equation and constrain the ν of interest that $\nu \gg \nu_{\rm p}$. To the lowest order of $\nu_{\rm p}/\nu$, the solution is

$$n(\nu) = 1+\frac{1}{2}\frac{1}{1-\beta\cos\theta}\left(\frac{\nu_{\rm p}}{\nu}\right)^2, \tag{5}$$

where ν is the frequency of the EMW, and the plasma frequency is

$$\nu_{\rm p} = \sqrt{\frac{e^2n'_{\rm e}}{\pi m_{\rm e}}} \approx 8.5\,{\rm kHz}\left(\frac{n'_{\rm e}}{{\rm cm}^3}\right)^{1/2}, \tag{6}$$

where $n'_{\rm e}$ is the electron number density in the stream comoving frame.

The above derivations ignored the gravitational redshift of the gravity of pulsar B. The gravitational redshift $z(r) \sim r_s/(2r)$, which is $\ll 1$ in the region where we are interested. $r_s \equiv 2GM_B/c^2$ is the Schwarzschild radius of pulsar B.

For an isotropic pulsar wind, the electron number density in the barycentric frame at a distance r is

$$n_e(r) = \frac{L_{sd}}{4\pi\beta c^3 r^2 m_e(1+\sigma)\gamma}, \quad (7)$$

where L_{sd} is the spin-down power, and σ is the magnetization parameter, which is defined as the ratio between the energy fluxes in the Poynting flow and that in the particles, γ is the Lorentz factor of the bulk velocity of the wind. The energy in the pulsar wind transfers from the Poynting flow to $e^{\pm}$ outward gradually. As $r \to \infty$, all the energy in the pulsar wind is transferred to electrons, thus $\sigma \to 0$ and $\gamma \to \gamma_\infty$. Due to the conservation of electrons in the region far outside the magnetosphere, $(1+\sigma)\gamma\beta$ remains constant and equal to γ_∞ (where $\beta \to 1$),

$$n'_e = n_e/\gamma. \quad (8)$$

Cos θ in equation (5) is given by the cosine theorem:

$$\cos\theta = \frac{l - a\cos\alpha}{\sqrt{a^2 + l^2 - 2al\cos\alpha}}, \quad (9)$$

where the notations are defined in above paragraph and in the illustrating Fig. 1, and

$$\cos\alpha = -\sin\theta_\oplus \cos(\phi_\oplus - \varphi), \quad (10)$$

where φ and $\phi_\oplus$ are the true anomaly and the azimuthal angle of the observer from the periastron of pulsar B, respectively, and $\theta_\oplus$ is the polar angle of the observer from the normal vector of the orbital plane. In the above derivation of geometry relationship, we assume the trajectories of light are straight lines. It is because we constrain our treatment where the pulse from pulsar A will not be eclipsed by the magnetosphere of pulsar B. Therefore, the *Einstein* angle of light deflection $\theta_{\rm Einstein} = 2r_s/r \ll 1$, where $r_s \sim 10^5$ cm is the Schwarzschild radius of pulsar B, and r is the impact distance of the light rays, which should be larger than the radius of the light cylinder (10^8 cm).

The time lag between a signal of infinity frequency and ν is

$$\delta t = \int_0^\infty \frac{n(\nu)\mathrm{d}l}{c\sqrt{1-r_s/r}} - \int_0^\infty \frac{\mathrm{d}l}{c\sqrt{1-r_s/r}}, \quad (11)$$

where the factor $\sqrt{1-r_s/r}$ accounts for the time dilation of general relativity and dl is the distance element away from the pulsar. With equation (5), the extra DM due to the pulsar wind is

$$\delta\mathrm{DM} = \int_0^\infty \frac{1}{\sqrt{1-r_s/r}} \frac{n'_e}{(1-\beta\cos\theta)}\mathrm{d}l. \quad (12)$$

The above integration starts from the pulsar and goes to infinity where the density of electrons in the pulsar wind is zero.

3 APPLICATIONS TO EXISTING DOUBLE-PULSAR SYSTEMS

3.1 PSR J0737−3039A/B

PSR J0737−3039A/B is the only known system that both of its companions are radio active pulsars. The parameters of this system are (Kramer & Stairs 2008) as follows.

(i) Orbital inclination angle: 88.°69.

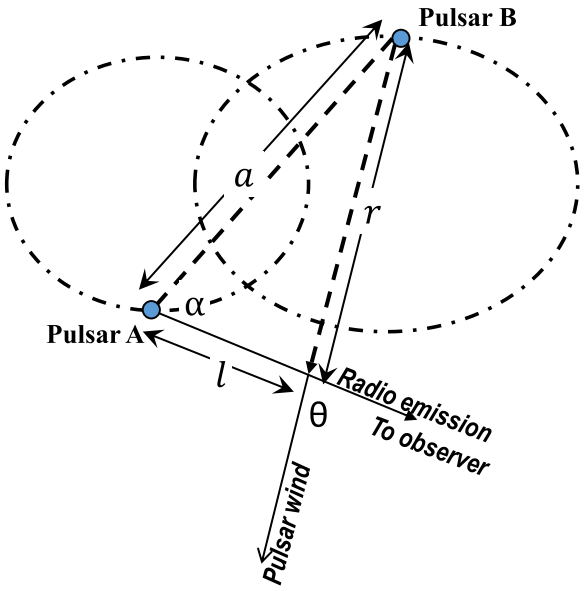

Figure 2. The definitions of angles and distances. Pulsar B is the source of the pulsar wind, and pulsar A is the source of radio signals to be observed.

(ii) Longitude of periastron: 87.°0331.
(iii) Eccentricity, $e = 0.087\,775$.
(iv) Projected semimajor axis, $x = (a/c)\sin i$:
pulsar A: 1.415 032 s; pulsar B: 1.5161 s.
(v) Spin-down luminosity of pulsar B, $L_{\rm sd,\,B} = 1.7 \times 10^{30}$ erg s^{-1}.

The bulk Lorentz factor of the pulsar wind as function of the distance is

$$\gamma(r) = \sqrt{1 + \left(\frac{\gamma_\infty}{1+\sigma(r)}\right)^2}, \quad (13)$$

where $\sigma(r)$ is described with equation (2), and

$$\sigma_L = \frac{B_L^2/8\pi}{2\dot{N}_{e^\pm} m_e c/r_L^2}, \quad (14)$$

where B_L is the magnetic field at the light cylinder, r_L is the radius of the light cylinder, $\dot{N}_{e^\pm} = N_m \dot{N}_{GJ}$, N_m is the multiplicity of $e^\pm$ and $\dot{N}_{GJ}$ is the Goldreich–Julian particle flow rate at the light cylinder. Kong et al. (2011) evaluated the σ_L of the Crab pulsar to be $\sim 10^5$.

With above parameters, we plot the δDM as function of the orbital phase (longitude from the ascending node) in Fig. 3, under different σ_L and α_σ. The orbital phases when pulsar A is eclipsed by the magnetosphere of pulsar B should be excluded from above Figs 2 and 3.

The additional DM causes delay of TOA of the pulses from pulsar A:

$$\Delta t = 4.15 \times 10^6\,\mathrm{ms} \times f^{-2} \times \delta DM, \quad (15)$$

where f is the radio frequency in which pulsar A is observed. Fig. 4 plots the Δt corresponding to δDM, when the observing frequency is 300 MHz.

When producing both of the figures, $\gamma_\infty = 10^3$ is adopted. As are shown in Figs 3 and 4, δDM and Δt increase towards the superior conjunction of pulsar A (when pulsar A is behind pulsar B). It is because that the path of signals from pulsar A is longer, with denser wind region in between the line of sight. In the cases of $\sigma_L = 10^3$, δDM and Δt also increase towards the inferior conjunction of pulsar A (when pulsar A is in front of pulsar B). It is because that

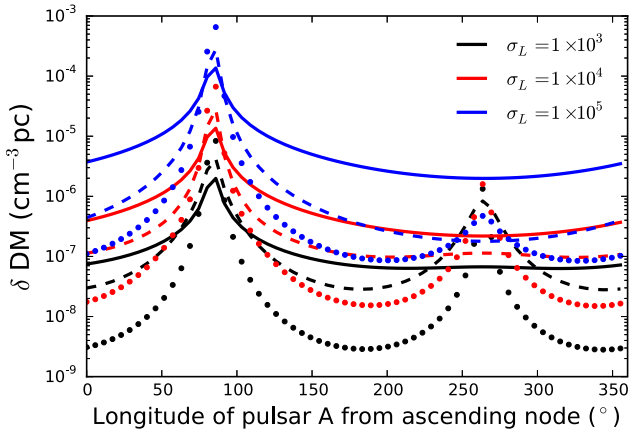

Figure 3. The additional DM in PSR J0737−3039A, under the assumptions of different $\sigma_{\rm L}$ and α_σ. The black, red and blue line colours (from bottom to top) correspond to $\sigma_{\rm L} = 1 \times 10^3$, 1×10^4 and 1×10^5, respectively. The solid, dashed and dotted line styles correspond to $\alpha_\sigma = 0$, 1, 2. For all curves, $\gamma_\infty = 10^3$ is adopted.

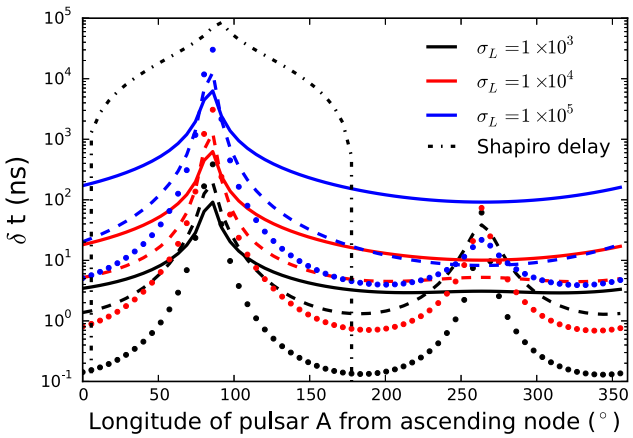

Figure 4. Time delay due to the additional DM in PSR J0737−3039A/B in the observing frequency of 300 MHz, compared with Shapiro delay (dash–dotted curve). The black, red and blue line colours (from bottom to top) correspond to $\sigma_{\rm L} = 1 \times 10^3$, 1×10^4 and 1×10^5, respectively. The solid, dashed and dotted line styles correspond to $\alpha_\sigma = 0$, 1 and 2, respectively. For all curves, $\gamma_\infty = 10^3$ is adopted.

with smaller $\sigma_{\rm L}$, the $e^\pm$ flow in the pulsar wind quickly becomes relativistic ($\beta \sim 1$). As a result, in the inferior conjunction where $\cos\theta \to 1$, the factor $1/(1 - \beta\cos\theta)$ increases significantly as $\beta \to 1$.

3.2 PSR J1915+1606 (B1913+16) as an example of DNS

PSR J1915+1606 (B1913+16), also known as the Hulse–Taylor binary, consists of two neutron stars. Only one of the neutron star is detected as a radio pulsar. The parameters of this system are (Weisberg & Huang 2016) as follows:

(i) Orbital inclination angle: 42.°84.
(ii) Longitude of periastron: 292.°544 50.
(iii) Eccentricity, $e = 0.617\,1340$.

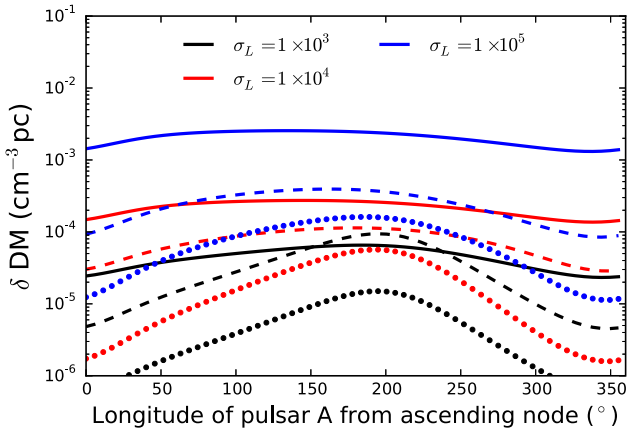

Figure 5. The additional DM of PSR J1915+1606, under the assumptions of different $\sigma_{\rm L}$ and α_σ. The black, red and blue line colours (from bottom to top) correspond to $\sigma_{\rm L} = 1 \times 10^3$, 1×10^4 and 1×10^5, respectively. The solid, dashed and dotted line styles correspond to $\alpha_\sigma = 0$, 1, 2. For all curves, $\gamma_\infty = 10^3$ is adopted.

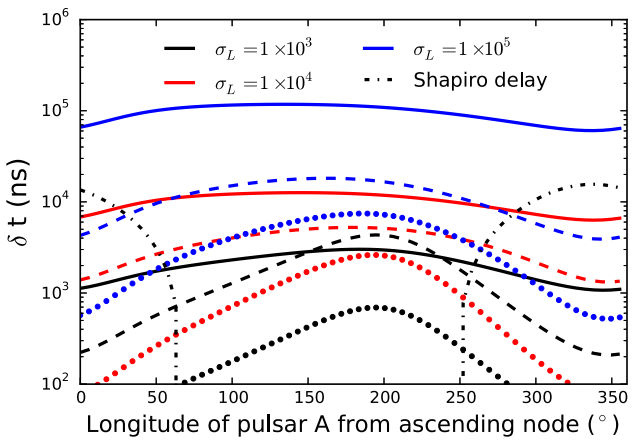

Figure 6. Time delay due to the additional DM in PSR J1915+1606 in the observing frequency of 300 MHz, compared with Shapiro delay (dash–dotted curve). The black, red and blue line colours (from bottom to top) correspond to $\sigma_{\rm L} = 1 \times 10^3$, 1×10^4 and 1×10^5, respectively. The solid, dashed and dotted line styles correspond to $\alpha_\sigma = 0$, 1 and 2, respectively. For all curves, $\gamma_\infty = 10^3$ is adopted.

(iv) Projected semimajor axis, $x = (a/c)\sin i = 2.341\,776$ s.
(v) Mass ratio between the pulsar and the companion neutron star: 1.0345.

We refer to the quite neutron star as 'pulsar B' although it is not detected as a pulsar. Since spin period and spin frequency derivative is not known, $r_{\rm L}$ and $L_{\rm sd}$ of it needs to be assumed. We assume $r_{\rm L}$ to be the same as PSR J0737−3039b, and $L_{\rm sd} = 10^{33}$ erg s^{-1} as a typical pulsar's spin-down luminosity. Besides, $\gamma_\infty = 10^3$ is adopted.

Similar with calculations in the case of PSR J0737−3039A/B, we plot δDM and Δt in Figs 5 and 6 with different $\sigma_{\rm L}$ and α_σ. Fig. 6 plots the corresponding time delay due to the additional DM in 300 MHz (see details in the caption of the figure). In contract with PSR J0737−3039A/B, the mild inclination angle (42.°84) and large eccentricity ($e = 0.617\,1340$) make the peaks of δDM and Δt

locate differently from that of the Shapiro delay, i.e. the superior conjunction.

4 FEASIBILITY OF ARCHIVAL, CURRENT AND FURTHER OBSERVATIONS

The best timing work of PSR J0737−3039A/B so far is Kramer et al. (2006). In that study, the pulsar was observed at six frequency bands of three large radio telescopes [64-m Parkes radio telescope, 76-m Lovell radio telescope and 100-m Green Bank Telescope (GBT)]. The observing frequencies range from 340 to 3030 MHz. The best timing precision of the pulsar A was obtained at 820 MHz of GBT, with typical TOA uncertainties of $18\,\mu\,s^{-1}$ with a 30-s integration.

From the analysis in the above section (see Fig. 4), in an optimistic case when $\sigma_L = 10^5$ and $\gamma_\infty = 10^3$, the predicted time delay is $\sim 10\,\mu\,s^{-1}$ at 300 MHz. At least four times longer integration of GBT data will be needed to improve the timing precision two times better than the current $\sim 18\,\mu s$. If the pulse profiles broadening towards low frequencies (either intrinsic or due to interstellar medium scattering) is taken into consideration (see fig. S.1 in Kramer et al. 2006), the integration should be longer up to ∼3 min. If we want to observe the signal as a function of orbital phase, the timing precision needs to be improved 20 times than current value. In this case, the integration needs to be as long as 5 h. Since the signal is orbital phase-dependent, we should not add up the data in different phases. Instead, we average the data in the same phase from different orbits. Observations of ∼20 orbits will be needed to obtain a resolution of 0.1 phase. In order to do that, a precious modelling of the peculiar evolution over orbits due to relativistic effects (Kramer 2014) is crucial.

Larger radio telescopes, e.g. FAST (Li & Pan 2016), SKA (Grainge et al. 2017), giving better timing precision and/or lower observing frequencies, e.g. LOFAR (Stappers et al. 2011), are helpful towards resolving the signals. We will study the further observational aspects using simulated observations in the following papers.

The spin-down luminosity of PSR J0737−3039A is ∼3000 times larger than the pulsar B. Thus, we expect the time delay of signals from pulsar B due to the pulsar wind of pulsar A could be ∼3000 times larger than that around, in the same observing frequencies. However, the emission of pulsar B is strongly influenced by the wind from pulsar A (Zhang & Loeb 2004), thus the pulse profiles are orbital phase-dependent (Burgay et al. 2005). Furthermore, there is a significant spin precession by $5.^\circ 1\,yr^{-1}$ (Burgay et al. 2005) as a result of general relativity coupling of spin and the total angular momentum (Damour & Ruffini 1974). Such orbital and secular evolution of the pulse profiles makes the timing precision of pulsar B much less than that of pulsar A (in Kramer et al. 2006, the rms timing residual of pulsar B with 300-s integration about 400 times larger than that of pulsar A).

The difficulties of observation in system PSR J0737−3039A/B are mainly due to the low spin-down luminosity of pulsar B. It is common to have $L_{sd} = 10^{33} \sim 10^{35}\,erg\,s^{-1}$ in pulsars. If in a DNS binary L_{sd} of the neutron-star companion is $10^{33} - 10^{35}\,erg\,s^{-1}$, the proposed features might have already been recorded in the archival data. As an example, the best up-to-date timing observation of PSR B1913+16 is done by Weisberg & Huang (2016). In their work, 31 yr of data from Arecibo Observatory at 1400 MHz were used. With 5-min integration, the TOA uncertainties were obtained as small as $\sim 5\,\mu s$. As shown in the above section (see Fig. 6), the predicted time delay may be ready to be seen ($10 - 20\,\mu s$) in an archival data in 300 MHz with the same timing precision, or at least a useful limit of the properties of the pulsar wind of the invisible neutron-star companion can be set from the data. The observation of the dispersive effects from the neutron-star companions provides a unique way to determine the pulsar nature of the invisible neutron stars, which cannot be probed otherwise.

5 SUMMARY

We studied the dispersive effects of the signal of a pulsar, arising from the pulsar wind of the other pulsar in a double-pulsar system. The resulted additional DM is formulated related to the properties of the pulsar wind. We applied the formula to the only known double-pulsar binary PSR J0737−3039A/B and the Hulse–Taylor binary as an example of potential intrinsic double-pulsar binaries. The conclusions of this work are listed below.

(i) Additional DM and the resulted time delay as functions of the orbital phase are able to reflect properties of the pulsar wind. These properties are: the spin-down luminosity L_{sd}, the magnetization parameter σ as a function of distance to the wind source, the asymptotic Lorentz factor of the $e^\pm$ in the wind γ_∞. See Figs 3–6.

(ii) For PSR J0737−3039A/B, the time delay in 300 MHz is $\lesssim 10\,\mu\,s^{-1}$ near the superior conjunction. The time delay is inversely proportional to the square of the observing frequencies. The current best timing accuracy of J0737−3039A is ∼2 times larger than wanted. Therefore, longer integration of data, further observations with larger telescopes and lower observing frequencies are needed.

(iii) With the assumption that the neutron-star companion of PSR B1913+16 has a typical spin-down luminosity of $10^{33}\,erg\,s^{-1}$, the time delay is as large as $10 - 20\,\mu\,s^{-1}$ in 300 MHz. The best timing precision of this pulsar is $\sim 5\,\mu\,s^{-1}$ in 1400 MHz. Therefore, it is possible that we can find this signal in archival data. Otherwise, we can set an upper limit on the spin-down luminosity to $\sim 10^{33}\,erg\,s^{-1}$, under certain assumptions of the pulsar wind properties.

6 DISCUSSION

The magnetosphere of PSR J0737−3039B is thought to be distorted by the wind from pulsar A (Lyutikov 2004). As a result, the wind from pulsar B should be anisotropic rather than what is assumed in this paper. However, we expected that the wind zone of pulsar B is less deformed, since the pulsar wind is lepton-dominated, and the interactions among leptons are weak. Besides, the spherically symmetric treatment above can serve as the zeroth-order approximation, before we can accurately model the directional dependence of the wind of pulsar B.

As can be seen from equations (7, 8 and 11), the amplitude of the proposed signal is proportional to L_{sd}/γ_∞^2. Therefore, if no such signal is seen, the upper limit will be actually set on the combination L_{sd}/γ_∞^2. The value of γ_∞ varies from 10^3 to 10^6 as fitted values in different models. $\gamma_\infty = 10^3$ is adopted throughout the calculations in this paper, as an optimized condition for the maximum TOA variation signals given L_{sd}. Larger γ_∞ will make the signal less likely to be seen.

ACKNOWLEDGEMENTS

We thank Prof. Kramer, Dr. Janssen and Prof. Lorimer for their instructive discussions on this idea. Prof. McLaughlin and Dr. Pol gave a lot of helpful suggestions on improving the manuscript. This work is partially supported by a GRF grant under 17302315.

REFERENCES

Aharonian F. et al., 2005, A&A, 442, 1
Arzoumanian Z. et al., 2016, ApJ, 821, 13
Babak S. et al., 2016, MNRAS, 455, 1665
Beskin V. S., 2016, in Aharonian F. A., Hofmann W., Rieger F. M., AIP Conf. Proc. Vol. 1792, High Energy Gamma-Ray Astronomy. Am. Inst. Phys., New York, p. 020001
Beskin V. S., Gurevich A. V., Istomin I. N., 1983, Zh. Eksp. Teor. Fiz., 85, 401
Beskin V. S., Kuznetsova I. V., Rafikov R. R., 1998, MNRAS, 299, 341
Bogovalov S. V., 1999, A&A, 349, 1017
Bogovalov S. V., 2001, A&A, 371, 1155
Bogovalov S. V., 2014, MNRAS, 443, 2197
Bogovalov S., Tsinganos K., 1999, MNRAS, 305, 211
Burgay M. et al., 2005, ApJ, 624, L113
Chernyakova M., Neronov A., Lutovinov A., Rodriguez J., Johnston S., 2006, MNRAS, 367, 1201
Chiueh T., Li Z.-Y., Begelman M. C., 1998, ApJ, 505, 835
Contopoulos I., Kazanas D., Fendt C., 1999, ApJ, 511, 351
Damour T., Ruffini R., 1974, C. R. Acad. Sci., Paris, 279, 971
Dubus G., 2015, C. R. Phys., 16, 661
Dubus G., Cerutti B., 2013, A&A, 557, A127
Grainge K. et al., 2017, Astron. Rep., 61, 288
Hirayama M., Cominsky L. R., Kaspi V. M., Nagase F., Tavani M., Kawai N., Grove J. E., 1999, ApJ, 521, 718
Hobbs G., Lyne A. G., Kramer M., 2010, MNRAS, 402, 1027
Hulse R. A., Taylor J. H., 1975, ApJ, 195, L51
Kennel C. F., Coroniti F. V., 1984, ApJ, 283, 694
Kirk J. G., Skjæraasen O., 2003, ApJ, 591, 366
Kirk J. G., Ball L., Skjæraasen O., 1999, Astropart. Phys., 10, 31
Kong S. W., Yu Y. W., Huang Y. F., Cheng K. S., 2011, MNRAS, 416, 1067
Kramer M., 2014, Int. J. Mod. Phys. D, 23, 1430004
Kramer M., Stairs I. H., 2008, ARA&A, 46, 541
Kramer M. et al., 2006, Science, 314, 97
Li D., Pan Z., 2016, Radio Sci., 51, 1060
Li L., Tong H., Yan W. M., Yuan J. P., Xu R. X., Wang N., 2014, ApJ, 788, 16
Lorimer D. R., Kramer M., 2012, Handbook of Pulsar Astronomy. Cambridge Univ. Press, Cambridge
Lyubarsky Y. E., 2002, MNRAS, 329, L34
Lyubarsky Y., Eichler D., 2001, ApJ, 562, 494
Lyutikov M., 2004, MNRAS, 353, 1095
Melatos A., Melrose D. B., 1996, MNRAS, 279, 1168
Michel F. C., 1969, ApJ, 158, 727
Spitkovsky A., 2006, ApJ, 648, L51
Stappers B. et al., 2011, in Burgay M., D'Amico N., Esposito P., Pellizzoni A., Possenti A., eds, AIP Conf. Proc. Vol. 1357, Radio Pulsars: An Astrophysical Key to Unlock the Secrets of the Universe. Am. Inst. Phys., New York, p. 325
Tong H., 2016, Sci. China Phys. Mech. Astron., 59, 5752
Tong H., Xu R. X., Song L. M., Qiao G. J., 2013, ApJ, 768, 144
Usov V. V., 1975, Ap&SS, 32, 375
Weisberg J. M., Huang Y., 2016, ApJ, 829, 55
Yang Y.-Y., Zhang C.-M., Li D., Wang D.-H., Pan Y.-Y., Lingfu R.-F., Zhou Z.-W., 2017, ApJ, 835, 185
Yi S.-X., Cheng K. S., 2017, ApJ, 844, 114
Yi S.-X., Zhang S.-N., 2016, Sci. China Phys. Mech. Astron., 59, 95
Zhang B., Loeb A., 2004, ApJ, 614, L53
Zhu X.-J., Wen L., Xiong J., Xu Y., Wang Y., Mohanty S. D., Hobbs G., Manchester R. N., 2016, MNRAS, 461, 1317

This paper has been typeset from a TEX/LATEX file prepared by the author.